Biosensors and Bioelectronics 105 (2018) 226–235

Contents lists available at ScienceDirect

Biosensors and Bioelectronics

journal homepage: www.elsevier.com/locate/bios

# Novel tungsten phosphide embedded nitrogen-doped carbon nanotubes: A portable and renewable monitoring platform for anticancer drug in whole blood

Haifeng Zhou[a], Guoxia Ran[a], Jean-Francois Masson[b], Chan Wang[a], Yuan Zhao[a], Qijun Song[a,*]

[a] Key Laboratory of Synthetic and Biological Colloids, Ministry of Education, School of Chemical and Material Engineering, Jiangnan University, Wuxi, Jiangsu 214122, China

[b] Department of Chemistry, Université de Montréal, C.P. 6128 Succ. Centre-Ville, Montreal, Quebec, Canada H3C 3J7

ARTICLE INFO

*Keywords:*
Biosensor
Anticancer drug
Tungsten phosphide
Nitrogen doped carbon nanotubes
Point-of-care testing

ABSTRACT

Biosensors based on converting the concentration of analytes in complex samples into single electrochemical signals are attractive candidates as low cost, high-throughput, portable and renewable sensor platforms. Here, we describe a simple but practical analytical device for sensing an anticancer drug in whole blood, using the detection of methotrexate (MTX) as a model system. In this biosensor, a novel carbon-based composite, tungsten phosphide embedded nitrogen-doped carbon nanotubes (WP/N-CNT), was fixed to the electrode surface that supported redox cycling. The electronic transmission channel in nitrogen doped carbon nanotubes (N-CNT) and the synergistic effect of uniform distribution tungsten phosphide (WP) ensured that the electrode materials have outstanding electrical conductivity and catalytic performance. Meanwhile, the surface electronic structure also endows its surprisingly reproducible performance. To demonstrate portable operation for MTX sensing, screen printing electrodes (SPE) was modified with WP/N-CNT. The sensor exhibited low detection limits (45 nM), wide detection range (0.01–540 μM), good selectivity and long-term stability for the determination of MTX. In addition, the technique was successfully applied for the determination of MTX in whole blood.

## 1. Introduction

The rapid development of highly electrocatalytic materials that are able to meet on-site fast response monitoring and inexpensive detection costs have prompted researchers to improve or redesign biosensors (Kimmel et al., 2012; Turner, 2013). For example, the field of clinical diagnostics and treatment especially requires sensors for monitoring drug levels in patients (McKeating et al., 2016). Hence, there is an urgent need to obtain accurate test results in a short time for a large number of samples to assist the doctor to decide on the course of medical treatments (Ronkainen et al., 2010). In addition, in vivo and real-time monitoring of anticancer drug concentration in plasma of patients will improve treatments, provided the availability of sensors. More importantly, frequent monitoring can avoid toxic effects and damage to organs (Cohen, 2000). Developing sensors for drug monitoring is important in the sensing community.

Methotrexate (MTX) is used worldwide in the treatment of a number of cancers and belongs to the class of antifolates. In addition, it is also frequently used to treat some autoimmune diseases, such as rheumatoid arthritis, psoriasis and lupus, because it has effective anti-inflammatory and immunosuppressive properties (Asadian et al., 2017). However, excessive use of MTX in clinical treatment can cause serious toxic side effects such as lung and liver disease, ulcerative stomatitis and low white blood cell counts (Rozenszajn and Radnay, 1974). Therefore, monitoring the concentration of MTX in blood is necessary in order to create an optimized dosage and thereby minimize the toxicity.

Current MTX detection methods focus on the use of modern instruments such as high performance liquid chromatography (HPLC), (Merás et al., 2005) fluorimetry, (Chen et al., 2007) UV–vis spectrophotometry, (Sastry and Lingeswara Rao, 1996) electrospray ionization tandem mass spectrometry (ESI-MS), (Barbieri et al., 2006) surface plasmon resonance (SPR) sensing (Zhao et al., 2015) and capillary electrophoresis (CE) (Szakács and Noszál, 2006). These techniques have the advantages of sensitivity and accuracy, meanwhile, they share some common drawbacks, such as high cost and tedious sample preparation method, which make them not suitable for continuous monitoring. In this regard, electrochemical methods with respect to their advantages such as simplicity, sensitivity, accuracy and ease of on-site applications have received considerable attention in recent years (Asadian et al., 2017). However, to the best of our knowledge, most of the research is

* Corresponding author.
*E-mail address:* qsong@jiangnan.edu.cn (Q. Song).

https://doi.org/10.1016/j.bios.2018.01.045
Received 15 November 2017; Received in revised form 31 December 2017; Accepted 21 January 2018

focused on the development of high-performance electrode materials or the improvement of the electrochemical sensors property. There is still a need for the miniaturization of MTX sensors for portable, reusable, and point-of-care testing.

Tungsten phosphide ($WP_2$ and WP) and its composite materials, an important family of catalysts, are beneficial for hydroprocessing catalysts (Clark et al., 2002; Li et al., 2017) and hydrogen evolution reaction (HER) (McEnaney et al., 2014; Xing et al., 2014). Obviously, $WP_2$ and WP have such a wide range of applications mainly due to their high electrical conductivity (Xing et al., 2014). In addition, support materials exhibit great influence on the cost, performance, and durability of electrocatalysts (Shao et al., 2009). Micro-nanostructured carbon materials, such as carbon black (Shu and Oyama, 2005), nitrogen-doped carbon matrix (Pu et al., 2016), and carbon cloth (Pu et al., 2014) among others, are important classes of novel support materials for WP mainly because their superior conductivity can significantly promote electrocatalytic performance. Furthermore, carbon nanotubes (CNT) and nitrogen-doped carbon nanotubes (N-CNT) are extremely important carbon-based supporting materials. Their unique structural, electrical, and mechanical properties were employed as novel composite materials with superior performance (Collins et al., 1997; Kang et al., 2009). Unfortunately, high-performance electrode materials that reasonably combine these two excellent species, WP and N-CNT, have not yet been reported. Meanwhile, these unique electron conduction rates and high electrocatalytic activity using for electrochemical sensors have also not been reported. Therefore, exploring the simple and reliable method of preparation WP modified N-CNT (WP/N-CNT) and developing high-performance electrochemical sensors based on this material is of great significance.

Here, a facile method to fabricate WP embedded nitrogen-doped carbon nanotubes via a two-step reaction was designed, and we report a sensor suited for on-site detection for the anticancer drug MTX. The uniform distribution of WP and the synergistic effect of N-CNT as electronic transmission channel ensured that the proposed sensor had superior sensing performance with a short response time, wide detection range, low detection limits, satisfactory selectivity and reproducibility for detection of MTX in whole blood. Finally, good performance and ease of use were obtained with the combination of WP/N-CNT with SPE, demonstrating its applicability to analyze small sample volumes and point-of-care testing (Fig. 1a).

## 2. Experimental section

### 2.1. Materials and Chemicals

Dopamine hydrochloride, multi-walled carbon nanotubes (CNT), tris(hydroxymethyl)aminomethane (Tris), ethanol, sodium hypophosphite, and tungsten chloride were purchased from Aladdin (Shanghai, China). Nitric acid (65%), $Na_2HPO_4$, and $NaH_2PO_4$ were purchased from Sinopharm Chemistry Reagent Co., Ltd. (Shanghai, China). Nafion (5%) and methotrexate were obtained from Sigma-Aldrich. All of the chemicals were analytical grade and used directly without further purification. Human blood was provided by the Affiliated Hospital of Jiangnan University and the 4th People's Hospital of Wuxi (Jiangsu, China). A SPE consisting of a carbon working electrode, a carbon counter electrode, and an Ag/AgCl reference electrode (Zensor R&D, Taiwan) was used for designing of portable electrochemical sensors. The deionized water was purified by a Millipore-Q system (Millipore Co., USA) and used for all aqueous solution preparation. As the supporting electrolyte, phosphate buffer (PB, 0.1 M) solution was prepared with $NaH_2PO_4$ and $Na_2HPO_4$.

### 2.2. Fabrication of WP/N-CNT modified GCE and SPE

Prior to modification, the bare GCE was successively polished to a mirror finish with 1, 0.3, and 0.05 μm alumina slurry, then sonicated successively with anhydrous alcohol and double-distilled deionized water, and dried with a $N_2$ stream. An amount of 2 mg WP/N-CNT (Detailed synthesis process can be seen in Supporting Information) was dispersed in a solution containing 100 μL water, 100 μL ethanol, and 0.05 wt% nafion. Then, the as-prepared WP/N-CNT solution (0.01 mg $mL^{-1}$, 10 μL) was cast onto the pretreated bare GCE or SPE surface and dried at room temperature. The electrode was noted as WP/N-CNT/GCE or WP/N-CNT/SPE.

### 2.3. Electrochemical measurement

Differential pulse voltammetry (DPV), cyclic voltammetry (CV) and chronoamperometric (CA) experiments were performed with an Electrochemical Analyzer (Model: 120C, S/N: uEA120C10001, Homiangz LLC) at room temperature. The GCE or modified GCE, platinum wire, and Ag/AgCl (KCl saturated) were served as working, counter and reference electrodes, respectively. For other experiments, a SPE was fixed on the electrode holder, and 25–30 μL of the sample was deposited on the surface of the three electrodes for detection. The DPV, and CV measurements were conducted in a PB solution (0.1 M, pH 4.0–9.0), and the voltage scanned from 0.4 to 1.0 V.

## 3. Results and discussion

### 3.1. Characterization of WP/N-CNT

The structure of the WP/N-CNT samples were observed with SEM. As shown in Fig. 1b, the CNT was coated with polydopamine (PDA), which is used as a unique supporting material for the adsorption and reduction of tungsten ions, while maintaining good dispersion of CNT. Then, high magnification SEM images further revealed that the surface of the WP/N-CNT was very rough and the diameter increased significantly (Fig. 1c). The TEM images of WP/N-CNT are shown in Fig. 1d and e. The multilayer structures was clearly observed, which proved that the PDA layer, approximately 12.18 nm, was successfully coated on the surface of the CNT. Meanwhile, tungsten trioxide was self-reduced and oxidized by the PDA layer. The formation of tungsten phosphide embedded nitrogen doped carbon was then realized through the high temperature calcination and phosphating treatment. Fig. 1f shows the TEM and corresponding EDX elemental mapping images, further indicating both P, W, N, C and O elements are uniformly distributed throughout the whole nanotubes. All these observations provide strong evidence to support the successful chemical conversion of CNT-PDA-$WO_3$ into WP/N-CNT after phosphating reaction. Especially, in-situ nitrogen doped carbon nanotubes (N-CNT) as an excellent electron transport channel greatly improved the electrochemical performance of electrode materials (Hueso et al., 2007). The introduction of WP on the surface layer could further enhance electrical conductivity and electrocatalytic properties.

The X-ray diffraction (XRD) patterns for CNT-PDA-$WO_3$ and WP/N-CNT were shown in Fig. 2a. As can be seen, the CNT-PDA-$WO_3$ shows the characteristic diffraction peaks of hexagonal-phase $WO_3$ (JCPDS No. 01–0486). After phosphating, the XRD pattern of WP/N-CNT could be clearly distinguished from the starting material as a series of diffraction peaks appeared as (110), (111), (121), (221) and (311) for WP, as well as diffraction peaks ascribed to (001), (200), (202), (002), (110), (201) and (311) for $WP_2$ according to PDF card (JCPDS No. 01-089-4778 and 01-076-2365). The diffraction peaks were sharp and intense, indicating that the WP/N-CNT was obtained with high purity and good crystallinity, which was also in agreement with the results of TEM and corresponding EDX elemental mapping. The morphological and structural characterization of the WP/N-CNT prompted us to make a structural model to reveal electrochemical properties derived from the structure and constituent. As shown in Fig. 2b, two characteristic peaks (D and G peaks) of graphitized carbon (1346 and 1575 $cm^{-1}$) were observed in the Raman spectrum of WP/N-CNT ($I_D/I_G$ = 0.91) and

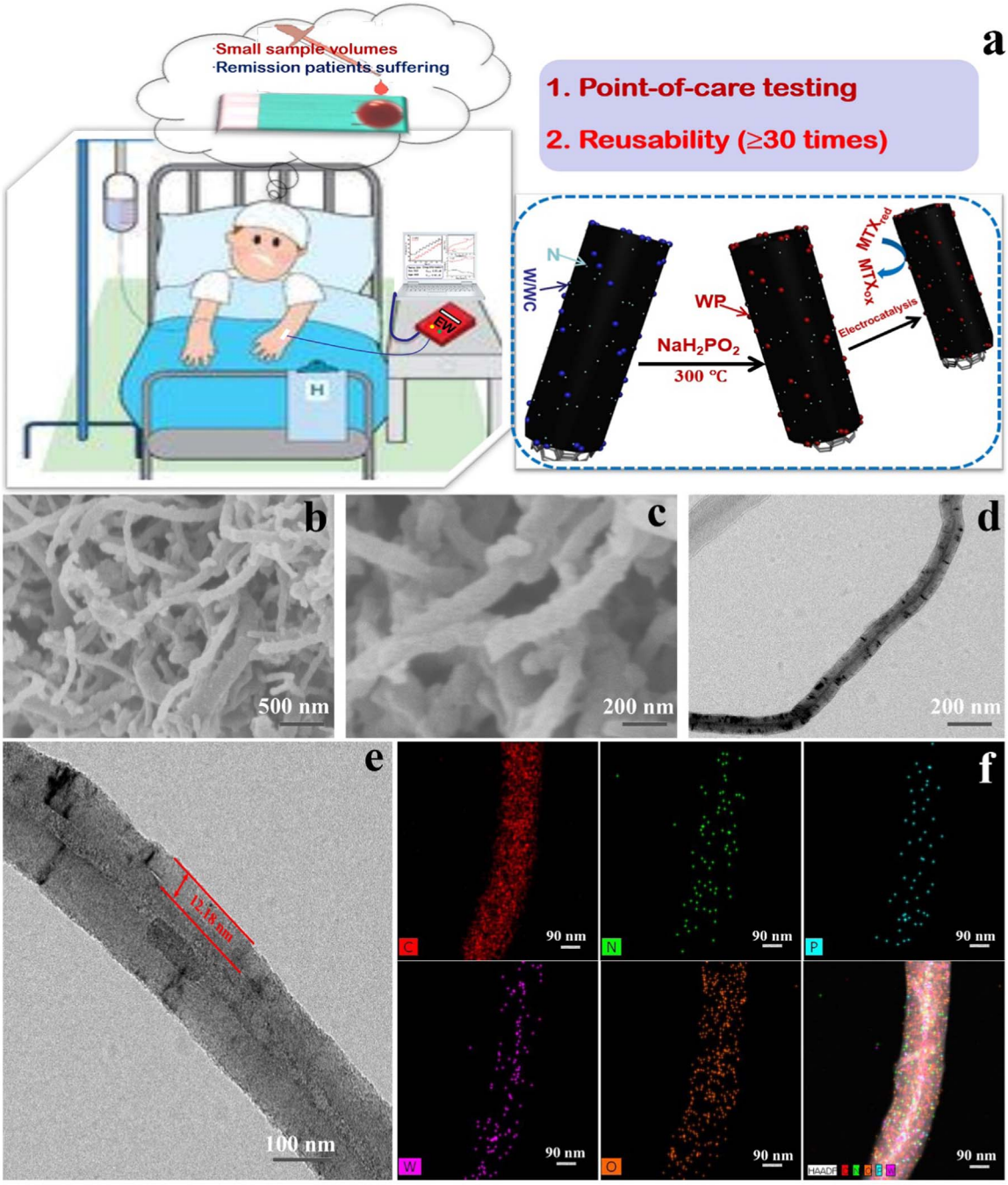


**Fig. 1.** (a) Schematic illustration of portable and renewable monitoring platform for anticancer drug (b, c) SEM images of the WP/N-CNT. (d, e) TEM image of the WP/N-CNT. (f) TEM EDX elemental mapping of C, N, P, W and O for the WP/N-CNT.

CNT-PDA-$WO_3$ ($I_D/I_G$ = 1.12). The ratio of intensities (the D and G bands) increased during the reduction and functionalization (Stankovich et al., 2007). Otherwise, the results demonstrated that labile oxygen-containing functional groups were pyrolysized with the increase of the carbonization temperature. Furthermore, the intensity and position of the second-order Raman band (2D) were an indicator to distinguish the number of layers of graphene and discriminate between electron and hole doping (Das et al., 2008; Graf et al., 2006; Jiao et al., 2009). As shown in Fig. 2b, it was observed that the 2D peak intensity was significantly increased and the positional decrease was shifted, which was due to the conversion of the PDA layer to the graphitized layer after high temperature calcination and increasing electron concentration in the system (Das et al., 2008). Thus, the use of WP/N-CNT as the electrochemical sensor material could exhibit multi-active sites, outstanding electrical conductivity and catalytic activity and specific response to the target analyte.

X-ray photoelectron spectroscopy (XPS) and energy-dispersive X-ray spectroscopy (EDS) results indicated that the WP/N-CNT were composed of C (90.2%), O (3.6%), N (0.7%), P (0.5%), and W (5.0%) (Fig. 1c-f and Fig. S1 a-c). Fig. 2d shows the W 4 f binding energy curves of WP/N-CNT. The three components including WC, W 4 $f_{5/2}$, and W $4f_{7/2}$ were derived by decomposing W 4f peaks. The W $4f_{5/2}$ peak at around 35.8 eV corresponds to $W^{\delta+}$ in WP, while the W $4f_{7/2}$ peak at around 37.9 eV corresponds to the $W^{6+}$ species (such as $WO_3$) (Wang et al., 2016b). Because the precursor of WP/N-CNT samples forms W° through the self-reduction of the PDA layer, and it is easy to react with the oxygen in the air. So, the existence of the peaks corresponding to tungsten oxide in the spectra was not surprising. The WC species

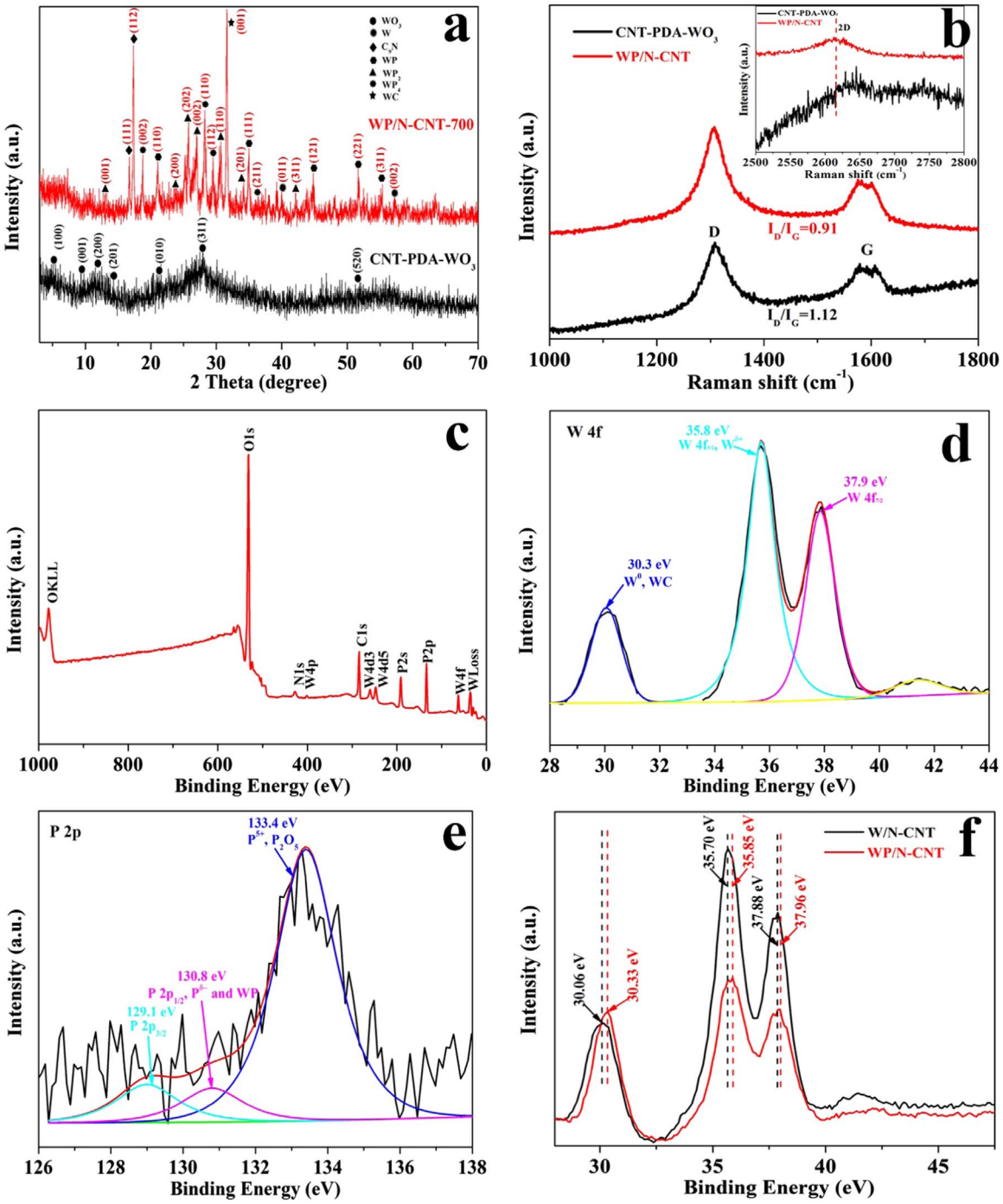


**Fig. 2.** (a) XRD patterns for CNT-PDA-$WO_3$ and WP/N-CNT-700. (b) Raman spectra for CNT-PDA-$WO_3$ and WP/N-CNT. Inset: 2D-band spectrum of the CNT-PDA-$WO_3$ and WP/N-CNT. (c-e) XPS total spectrum and XPS spectra in the W and P regions of WP/N-CNT. (f) W 4 f of W/N-CNT versus WP/N-CNT.

formed in this process should play a certain role in enhancing the adhesion between WP and the carbon substrate (Oyama et al., 2002). However, diffraction peaks of WC were not significantly observed in the XRD spectra, suggesting that the content of WC species was negligible in WP/N-CNT composites. Except for tungsten oxide and WC, other W species were not found in the XPS spectra, suggesting that most W was reacted with P to generate WP (Duan et al., 2016). The high-resolution P 2p region (Fig. 2e) showed two peaks at 133.4 eV and 130.8 eV, reflecting the binding energy of $P^{5+}$ and $P^{\delta-}$, respectively, along with one peak at 129.1 eV (Pu et al., 2014). The typical peak of $P^{5+}$ species ($P_2O_5$) could be observed in WP/N-CNT, indicating that phosphorus oxides originating from the oxidation process inevitably exist on the composite surface.

The presence of $W^{\delta+}$ and $P^{\delta-}$ species confirmed the successful synthesis of WP in the carbon skeleton, which could act as the active sites for the electrocatalytic reaction. Specifically, methotrexate belongs to pteridine groups, and the amino group at the C2 position on the pyrimidine ring is electroactive (Gao et al., 2007; Gorren et al., 2001). Thus, an intermediate of positive nitrogen free radical could be formed under the action of the active site of the electrode material. And the free radical could undergo polymerization and form insoluble products that deposit on the electrode surface, which agrees with the phenomena of recorded voltammetric behaviors (Scheme S1) (Gao et al., 2007). In addition, XPS spectrum of N 1 s peaks disclosed that the amino-type

nitrogen from PDA was completely transformed into pyridinic N (398.8 eV), pyrrolic N (400.3 eV), graphitic N (401.4 eV), and oxidized N (402.4 eV) in WP/N-CNT (Fig. S1a). This indicated that the nitrogen atoms were doped in the carbon nanotubes, which ensured that the electrode material had excellent conductivity. As can be seen in Fig. S1b, three components at around 284.3, 286.1, and 288.5 eV in the C 1 s spectra correspond to the C-C, C-N/C=N and O=C-O, respectively. Formation of graphitic carbon in WP/N-CNT is important for enhancing the electrical conductivity, which is expected to improve the performance of the sensor. Furthermore, four different peaks could be observed from the O 1s spectra (Fig. S1c), which correspond to the physically absorbed O or carbonates (530.8 eV), O-P (531.4 eV), C-O-C/C-O-H/C-OH (533.1 eV), and W-O (535.7 eV). As shown in Fig. 2f, compared with CNT-PDA-$WO_3$, the W 4f peaks of WP/N-CNT were shifted to a higher binding energy, confirming that the oxidation state was increased. This could be explained from the formation of metal phosphides (Jin et al., 2016).

### 3.2. Electrochemical behavior of WP/N-CNT

The CV and electrochemical impedance spectra (EIS) of the modified electrodes were acquired with the redox probe 5.0 mM $Fe(CN)_6^{3-/4-}$ containing 0.1 M KCl (Fig. 3a and b). By fitting the data with Randles equivalent circuit (Fig. 3b-I), the electron transfer resistance of the probe was 51.2, 34.5, 13.3, 11.8 and 8.2 Ω at the CNT-PDA-$WO_3$/GCE, W/N-CNT-700/GCE, GCE, WP/N-CNT-800/GCE and WP/N-CNT-700/GCE, respectively. For the WP/N-CNT-700/GCE, the Nyquist plot appeared to have a small diameter, demonstrating relatively lower electron transfer resistance of the probe. This observation demonstrated the advantage of phosphating and the appropriate calcination temperature to improve the electrochemical performance.

The electrochemistry of MTX in PB (pH 6.0) was thereafter investigated at a bare GCE, CNT-PDA-$WO_3$/GCE, W/N-CNT-700/GCE, WP/N-CNT-800/GCE and WP/N-CNT-700/GCE. The WP/N-CNT-700/GCE showed superior electrocatalytic activity toward the MTX, as a significant increase in oxidation current was observed (Fig. 3c). When compared to WP/N-CNT-700/GCE, the CNT-PDA-$WO_3$/GCE and W/N-CNT-700/GCE showed weak Faradaic responses for MTX at the potential range from 0.4 to 1.0 V (Fig. 3d). These results demonstrated the superior performance of WP/N-CNT-700/GCE, suggesting an electroactive interface with high electrochemical activity was obtained through the WP modification. Thus, the WP/N-CNT-700 was selected as the best electrode material for the preparation of the sensor for subsequent experiments. On the other hand, the above results also suggested that a potential range of 0.4–1.0 V was appropriate for the DPV method.

### 3.3. Effect of scan rate and pH on the electrocatalytic oxidation of MTX

To understand the charge transfer characteristics of MTX on modified electrodes, we respectively recorded CVs of MTX on WP/N-CNT/GCE in PB (pH 6.0) at various scan rates ($\nu$). From the CVs as displayed in Fig. 4a, the oxidation of MTX was completely irreversible. The oxidation peak current ($I_{pa}$) for MTX was directly proportional to the scan rate in the studied ranges (Fig. 4b). The result indicated that the electrode reaction of MTX on WP/N-CNT/GCE is an adsorption-controlled

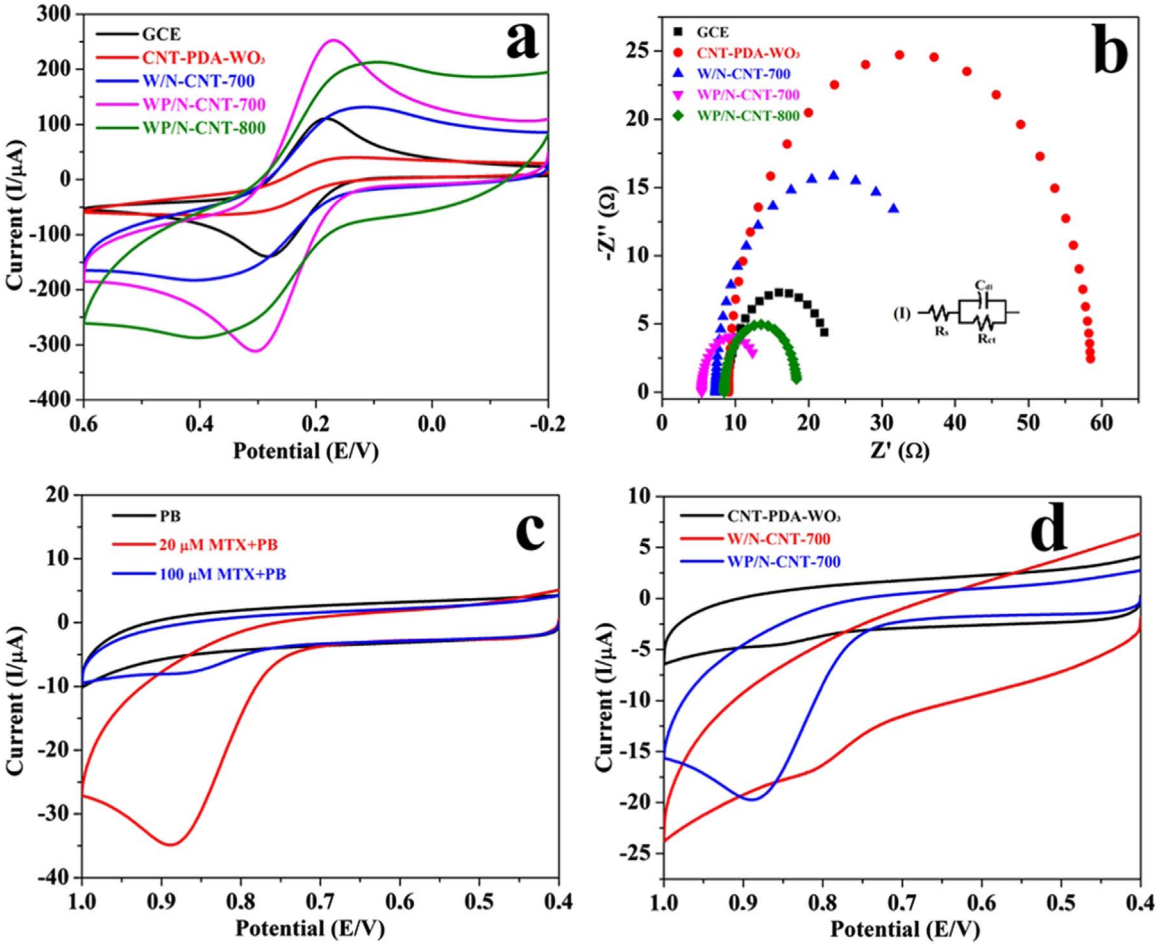


**Fig. 3.** (a) (b) CV and EIS plots of 5.0 mM $[Fe(CN)_6]^{3-/4-}$ containing 0.1 M KCl recorded with different electrodes, Inset: Randle's equivalent circuit model for the impedance data. (c) CVs of WP/N-CNT/GCE in PB containing 20 and 100 μM MTX. (d) CVs of CNT-PDA-$WO_3$/GCE, W/N-CNT-700/GCE, and WP/N-CNT-700/GCE in PB.

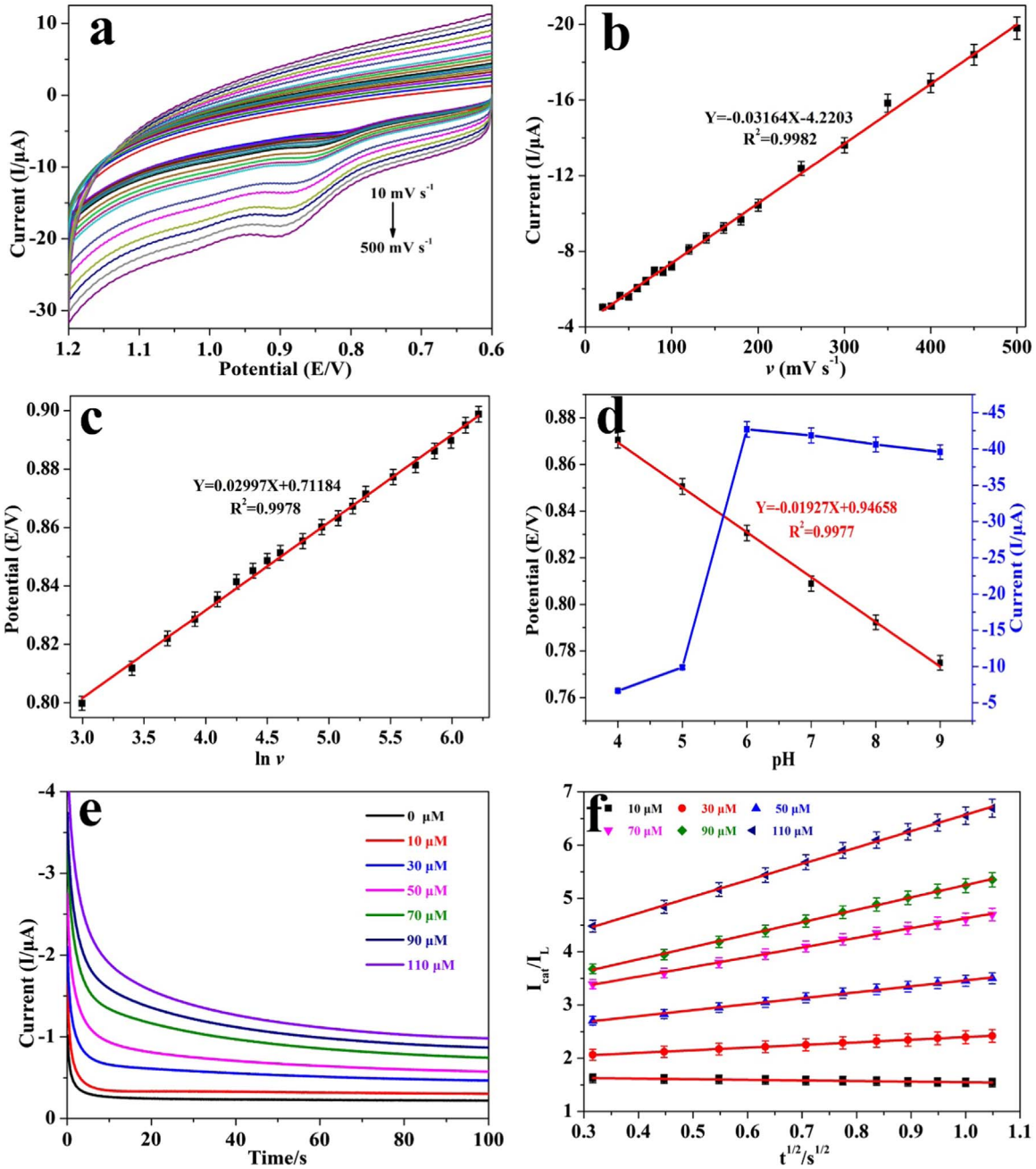


**Fig. 4.** (a) CVs of 0.1 mM MTX at WP/N-CNT/GCE at different scan rates from 0.01 V $s^{-1}$ to 0.5 V $s^{-1}$. (b) Variation of the peak currents versus scan rate ($\nu$). (c) The relationships of peak potentials ($E_p$) versus ln $\nu$. (d) The peak currents of MTX (0.1 mM) in PB solution with WP/N-CNT/GCE at different pH value, and variation of the peak potentials versus pH. (e) CA of WP/N-CNT/GCE in PB upon adding increasing amounts of MTX at 0.77 V. (f) Plots of $I_{cat}/I_L$ versus $t^{1/2}$ at different MTX concentrations.

processes, which demonstrated that the current waves were due to the oxidation of the adsorbed MTX.

For an adsorption-controlled and totally irreversible electrode process, the peak potential ($E_{pa}$) is related to the scan rate ($\nu$) by the equation.

$$E_{pa} = E^{0'} - \left(\frac{RT}{\alpha nF}\right)\ln\left(\frac{RTk_s}{\alpha nF}\right) + \left(\frac{RT}{\alpha nF}\right)\ln\nu$$

From the relationship of $E_{pa}$ versus $\nu$ as shown in Fig. S2, the value of $E^{0'}$ is estimated to be 0.81 V via extension of the curve to $\nu = 0$. Then, from the plot of $E_{pa}$ versus ln $\nu$ as displayed in Fig. 4c. Thus, according to slope and intercept of regression equation, the values of the transfer coefficient ($\alpha$) and standard electron transfer rate constant ($k_s$) were calculated to be 0.43 and 0.938 $s^{-1}$, respectively. This $k_s$ value is twice that of MWCNTs-DHP based sensor (0.46 $s^{-1}$), suggesting that the MTX have fast electron transfer kinetics on the developed sensing interface (Oliveira et al., 2013).

The electrochemical behavior of MTX is directly influenced by the pH of the supporting electrolyte, which will certainly affect the adsorption rates of MTX on the catalyst surface and, thus, the oxidation currents. To investigate the effect of the pH on the electro-oxidation of MTX at the WP/N-CNT modified electrode, CVs of 50 μM MTX were recorded at different pH values in the range of 4.0–9.0 (Fig. 4d). It was found that with the increase of pH value of the supporting electrolyte, the peak potential shifted negatively, suggesting the participation of protons in the oxidation reaction.

Furthermore, by raising the pH values from 4.0 to 6.0, the oxidation peak current of MTX gradually increased and reached maximum at pH

6.0. Further increase of the pH to 9.0 caused the peak height to decrease. Hence, PB of pH 6.0 was chosen as the optimum supporting electrolyte and used for all further experiments.

### 3.4. WP/N-CNT electrocatalytic oxidation for MTX

We have further investigated the electrochemical kinetic and electrocatalytic parameter of WP/N-CNT toward MTX using CA. Fig. 4e shows the CA response of 0.1 M PB pH 6.0 in the absence and presence of increasing concentrations of MTX at WP/N-CNT/GCE (constant potential 0.77 V). At intermediate time points, the current was dominated by the rate of the electron transfer toward the electrocatalytic oxidation of MTX. Thus, the catalytic rate constant ($K_{cat}$) can be calculated according to the following equation:

$$\frac{I_{cat}}{I_L} = (\pi K_{cat} C_0 t)^{1/2}$$

where $I_{cat}$ and $I_L$ are the currents of WP/N-CNT/GCE in presence and absence of MTX, respectively, and $K_{cat}$ is the catalytic rate constant. Clearly, the $I_{cat}/I_L$ versus $t^{1/2}$ relation is linear (Fig. 4f). From the slopes of $I_{cat}/I_L$-$t^{1/2}$, the average value of $K_{cat}$ is calculated to be $1.45 \times 10^5$ $M^{-1}$ $s^{-1}$, which is larger than the previously reported valuable electrode materials (Guo et al., 2011; Phal et al., 2017), confirming that the WP/N-CNT has a greater electrocatalytic activity for the oxidation of MTX.

### 3.5. Determination of MTX at WP/N-CNT/SPE

Based on the facile preparation of WP/N-CNT, excellent conductivity, unique electrocatalytic activity and high response to the MTX, we thus proposed a strategy to develop it as a portable monitoring platform that could be used for point-of-care testing with smaller sample size, as shown in Fig. 5a and b.

Under the optimal experimental conditions, DPV and CA of WP/N-CNT/SPE in 0.1 M PB (pH 6.0) containing different concentrations of MTX were recorded. The oxidation currents increased proportionally to the concentration of MTX (Fig. 5c). The calibration curve of the oxidation peak currents versus concentrations of MTX was linear (Fig. 5d). Then, based on signal-to-noise (S/N = 3) characteristic, the limit of detection (LOD) was estimated to be 45 nM, which is similar to a limit of detection of 28 nM found with SPR sensing (Zhao et al., 2015).

CA technology possesses the advantages of real-time monitoring and higher sensitivity than other techniques for quantitative analysis because it is achieved by applying an optimized applied potential ($E_a$) (Wang et al., 2016a). Therefore, in this work, the applied potential of the biosensor for the detection of MTX was also optimized. Fig. 5e presents a typical real-time amperometric *I-t* curve using WP/N-CNT/SPE with subsequent injection of various concentrations of MTX into PB solution under optimized applied potential (0.77 V). The corresponding calibration curve of catalytic current (*I*) versus MTX concentration (C) was then extracted. From the curves, three linear ranges were obtained over MTX concentration ranging from 0.01 μM to 250 μM (Fig. 5f).

In addition, the limit of detection (LOD) corresponding to three times the relative standard deviation (RSD) of the average blank value (LOD = 3 × RSD/Slope) was estimated to be 45 nM. The analytical performance of our sensor was comparable or better than those reported at other modified electrodes, and the results were listed in Table S1.

### 3.6. Interference studies

Selectivity is an important factor in evaluating the performance of electrochemical sensors. In this study, the effect of the possible interfering species on the detection of MTX was investigated by adding potentially interfering species into PB containing 20 μM MTX. As shown in Fig. 6a, the results illustrated that the common inorganic ions, such as $K^+$, $Na^+$, $Ca^{2+}$, $Mg^{2+}$, $Zn^{2+}$, $Fe^{2+}$, $Fe^{3+}$, $Cl^-$, $NO^{3-}$, and $SO_4^{2-}$ in 100-fold excess, did not significantly affect the response of the sensor (signal change below 5%). In addition, some biological molecules, such as glycine (Gly), cysteine (Cys), lysine (Lys), tryptophan (Trp), urea acid (UA), citric acid (CA), ascorbic acid (AA), dopamine (DA) (in 20-fold excess), glucose (in 50-fold excess) also had negligible interference on the determination of MTX (Fig. 6b). All these results suggested that the sensor has a satisfactory stability and high selectivity for determination of MTX.

### 3.7. Reusability and stability

Reusability and stability play an important role in the storage and application of sensors. In the course of the experiment, we confirmed that the electrodes still maintained with a significant oxidation peak, and the influence caused by the adsorption of reaction residues on the electrode surface could be overcome by running CV (7 times) or DPV (6 times) in a fresh PB solution (Fig. 6c and d). This is presumably due to the strong electrocatalytic performance of WP/N-CNT, which depleted the limited MTX adsorbed on the electrode surface. More importantly, an intermediate of positive nitrogen free radical belonging to MTX could undergo polymerization and form insoluble products that deposit on the electrode surface. However, the product was easily dispersed into the fresh PB solution, thereby cleaning the electrode surface. Meanwhile, the reproducibility of WP/N-CNT/SPE was evaluated by preparing independently five electrodes for the determination of MTX (Fig. 6e). The electrode was recycled 30 times and still maintained good performance, with the average standard deviations of current measurements below 5%. This result indicated that the sensor will significantly reduce the cost of testing. The stability of the modified electrode was also investigated. After the modified electrodes were kept at ambient temperature for 30 days, the peak signal was 97% of the original value for MTX. Therefore, we can declare that the developed biosensor has satisfactory stability and reproducibility.

### 3.8. Real sample analysis

The performance of the proposed sensor was verified with the detection of MTX in clinical samples. WP/N-CNT/SPE was further utilized to measure MTX in whole blood spiked with MTX. In short, the whole blood (20 μL) was diluted with 10 μL of PB solution (0.1 M, pH 6.0) and spiked with a standard solution of MTX, subsequently analyzed with the WP/N-CNT/SPE. The results are shown in Fig. 6f and Table S2. The MTX content in whole blood sample was calculated using a regression equation (Fig. 5d and f). The recoveries were in range of 98.5–100.3%, suggesting good feasibility and reliability of the proposed electrode for detection of MTX in whole blood.

## 4. Conclusion

This work provided a novel portable and reusable analytics platform based on tungsten phosphide embedded nitrogen-doped carbon nanotubes (WP/N-CNT) for electrochemical detection of MTX. The main conclusions of present work include: (1) A novel electrode material featured with multi-active sites, excellent electrical conductivity and electrocatalytic activity was designed and successfully prepared. The dispersed active sites were effectively connected by the electronic transmission channel, N-CNT. (2) WP/N-CNT nanocomposites was successfully synthesized through an environmentally-friendly approach and used to modify the working electrode. (3) An electrochemical method that requires small sample volumes and recyclable electrode was developed, which satisfies the need for point-of-care testing, and achieves faster, simpler and cheaper detection of MTX. The fabricated electrochemical sensor showed low detection limits, high sensitivity, wide linear ranges, good stability and reproducibility. This device would provide a new platform for low cost, portable, and point-of-care

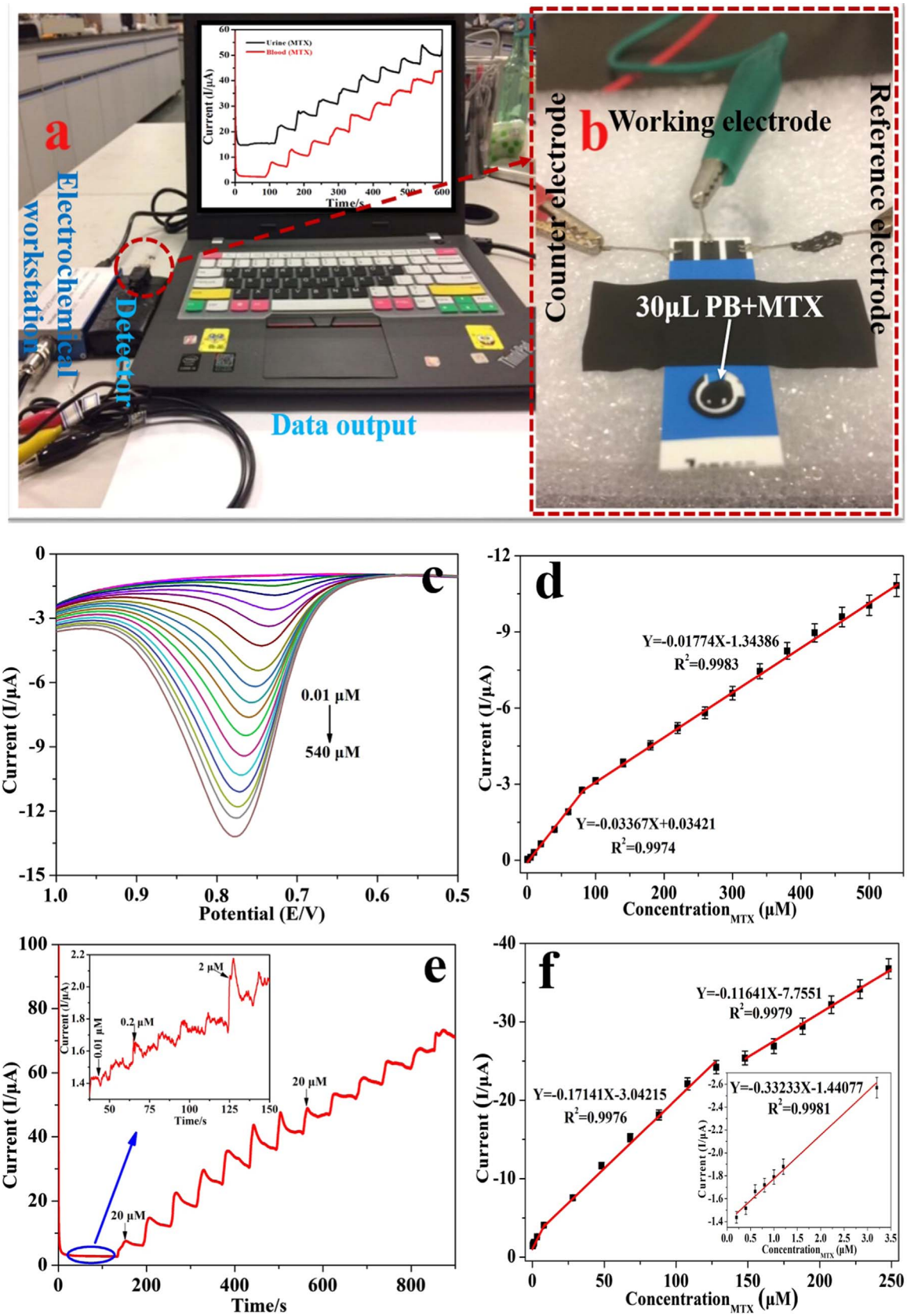


**Fig. 5.** (a) (b) Picture of the portable biosensor system. (Left) Dimensions of electrochemical analyzer: 100 (L) × 64 (W) × 24 (H) mm. Weight: 150 g. (Middle) The SPE is inserted into the USB port as sensor probe. (Right) The data output system is controlled by laptop. (c) DPVs of WP/N-CNT/SPE in PB containing a mixture of MTX; (d) the relationship of $I_{pa}$ versus the concentrations of MTX; (e) CA responses of the WP/N-CNT/SPE upon successive additions of MTX at the applied potential of 0.77 V. Inset is the amplified I−t curve in the low concentration region of MTX; (f) Calibration plots for the WP/N-CNT/SPE with MTX concentrations. The inset shows the calibration curve with MTX concentrations.

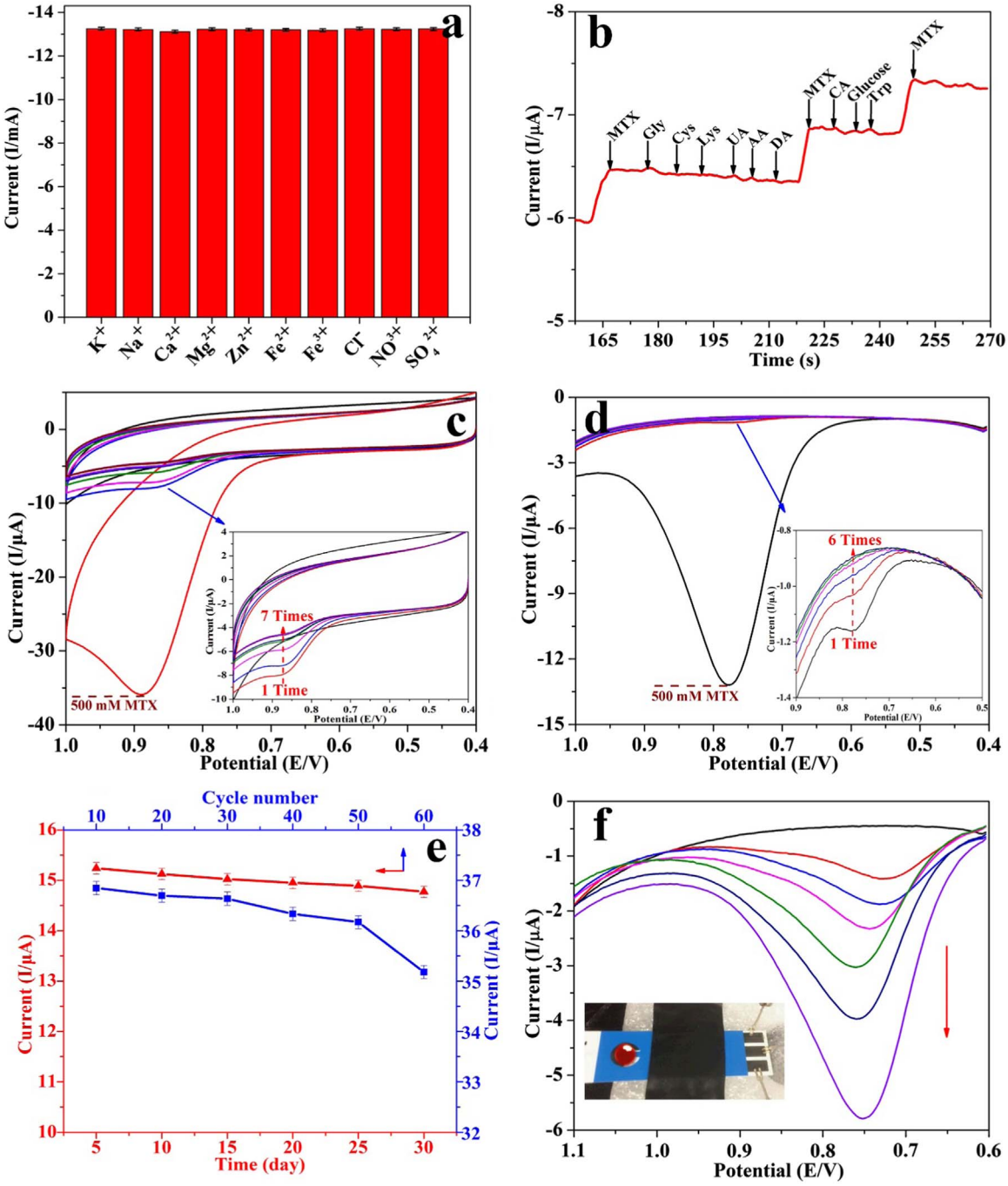


**Fig. 6.** (a) Inorganic ions interference of the WP/N-CNT/SPE for detection of MTX (b) CA responses of the WP/N-CNT/SPE after successive addition of MTX, Gly, Cys, Lys, UA, AA, DA, MTX, CA, Glucose, Trp, and MTX into PB at 0.77 V. (c) (d) The electrode was cleaned by CV and DPV methods; (e) Oxidation currents at various storage times and cycle numbers; (f) DPVs of WP/N-CNT/SPE in varied concentrations of standard addition of MTX.

testing to cancer treatment. Although anticancer drugs do not enable real-time and in situ monitoring in vivo, but the present work shows that the detection of in vitro samples is feasible. Hence it would be possible to fully resolve such problems by developing of novel micro/nanoelectrodes in future studies.

## Acknowledgments

This work was supported by the National Natural Science Foundation of China (Grant No. 51502115), the Enterprise university-research prospective program Jiangsu Province (BY 2015019-22), and the authors gratefully acknowledge financial support from China Scholarship Council and from the Natural Science and Engineering Research Council (NSERC) of Canada.

## Notes

The authors declare no competing financial interest.

## Appendix A. Supplementary material

Supplementary data associated with this article can be found in the online version at http://dx.doi.org/10.1016/j.bios.2018.01.045.

## References


Asadian, E., Shahrokhian, S., Zad, A.I., Ghorbani-Bidkorbeh, F., 2017. Sens. Actuators B 239, 617–627.

Barbieri, A., Sabatini, L., Indiveri, P., Bonfiglioli, R., Lodi, V., Violante, F.S., 2006. Rapid Communications in Mass Spectrometry, 20(12), pp. 1889–1893.

Chen, S., Zhang, Z., He, D., Hu, Y., Zheng, H., He, C., 2007. Luminescence 22 (4), 338–342.

Clark, P., Wang, X., Oyama, S.T., 2002. J. Catal. 207 (2), 256–265.

Cohen, M.R., 2000. BMJ: Br. Med. J. 320 (7237), 728.

Collins, P.G., Zettl, A., Bando, H., Thess, A., Smalley, R., 1997. Science 278 (5335), 100–102.

Das, A., Pisana, S., Chakraborty, B., Piscanec, S., Saha, S., Waghmare, U., Novoselov, K., Krishnamurthy, H., Geim, A., Ferrari, A., 2008. Nat. Nanotechnol. 3 (4), 210–215.

Duan, Y., Sun, Y., Pan, S., Dai, Y., Hao, L., Zou, J., 2016. ACS Appl. Mater. Interfaces 8 (49), 33572–33582.

Gao, L., Wu, Y., Liu, J., Ye, B., 2007. J. Electroanal. Chem. 610 (2), 131–136.

Gorren, A.C., Kungl, A.J., Schmidt, K., Werner, E.R., Mayer, B., 2001. Nitric Oxide 5 (2), 176–186.

Graf, D., Molitor, F., Ensslin, K., Stampfer, C., Jungen, A., Hierold, C., Wirtz, L., 2006. arXiv preprint cond-mat/0607562.

Guo, Y., Chen, Y., Zhao, Q., Shuang, S., Dong, C., 2011. Electroanalysis 23 (10), 2400–2407.

Hueso, L.E., Pruneda, J.M., Ferrari, V., Burnell, G., Valdés-Herrera, J.P., Simons, B.D., Littlewood, P.B., Artacho, E., Fert, A., Mathur, N.D., 2007. Nature 445 (7126), 410–413.

Jiao, L., Zhang, L., Wang, X., Diankov, G., Dai, H., 2009. Nature 458 (7240), 877–880.

Jin, Z., Li, P., Xiao, D., 2016. Green Chem. 18 (6), 1459–1464.

Kang, J., Zhang, S., Zhang, Q., Wang, Y., 2009. Angew. Chem. Int. Ed. 121 (14), 2603–2606.

Kimmel, D.W., LeBlanc, G., Meschievitz, M.E., Cliffel, D.E., 2012. Anal. Chem. 84 (2), 685.

Li, X., Tian, S., Wang, A., Prins, R., Li, C., Chen, Y., 2017. J. Catal. 352, 557–561.

McEnaney, J.M., Crompton, J.C., Callejas, J.F., Popczun, E.J., Read, C.G., Lewis, N.S., Schaak, R.E., 2014. Chem. Commun. 50 (75), 11026–11028.

McKeating, K.S., Aubé, A., Masson, J.-F., 2016. Analyst 141 (2), 429–449.

Merás, I.D., Mansilla, A.E., Gómez, M.J.R., 2005. Anal. Biochem. 346 (2), 201–209.

Oliveira, G.G., Janegitz, B.C., Zucolotto, V., Fatibello-Filho, O., 2013. Cent. Eur. J. Chem. 11 (11), 1837–1843.

Oyama, S.T., Clark, P., Wang, X., Shido, T., Iwasawa, Y., Hayashi, S., Ramallo-Lopez, J., Requejo, F., 2002. J. Phys. Chem. B 106 (8), 1913–1920.

Phal, S., Lindholm-Sethson, B., Geladi, P., Shchukarev, A., Tesfalidet, S., 2017. Anal. Chim. Acta 987, 15–24.

Pu, Z., Liu, Q., Asiri, A.M., Sun, X., 2014. ACS Appl. Mater. Interfaces 6 (24), 21874–21879.

Pu, Z., Ya, X., Amiinu, I.S., Tu, Z., Liu, X., Li, W., Mu, S., 2016. J. Mater. Chem. A 4 (40), 15327–15332.

Ronkainen, N.J., Halsall, H.B., Heineman, W.R., 2010. Chem. Soc. Rev. 39 (5), 1747–1763.

Rozenszajn, L., Radnay, J., 1974. Blood 43 (3), 401–409.

Sastry, C.S., Lingeswara Rao, J.S., 1996. Anal. Lett. 29 (10), 1763–1778.

Shao, Y., Liu, J., Wang, Y., Lin, Y., 2009. J. Mater. Chem. 19 (1), 46–59.

Shu, Y., Oyama, S.T., 2005. Carbon 43 (7), 1517–1532.

Stankovich, S., Dikin, D.A., Piner, R.D., Kohlhaas, K.A., Kleinhammes, A., Jia, Y., Wu, Y., Nguyen, S.T., Ruoff, R.S., 2007. Carbon 45 (7), 1558–1565.

Szakács, Z., Noszál, B., 2006. Electrophoresis 27 (17), 3399–3409.

Turner, A.P., 2013. Chem. Soc. Rev. 42 (8), 3184–3196.

Wang, Q., Yang, Y., Gao, F., Ni, J., Zhang, Y., Lin, Z., 2016a. ACS Appl. Mater. Interfaces 8 (47), 32477–32487.

Wang, X.-D., Xu, Y.-F., Rao, H.-S., Xu, W.-J., Chen, H.-Y., Zhang, W.-X., Kuang, D.-B., Su, C.-Y., 2016b. Energy Environ. Sci. 9 (4), 1468–1475.

Xing, Z., Liu, Q., Asiri, A.M., Sun, X., 2014. ACS Catal. 5 (1), 145–149.

Zhao, S.S., Bukar, N., Toulouse, J.L., Pelechacz, D., Robitaille, R., Pelletier, J.N., Masson, J.-F., 2015. Biosens. Bioelectron. 64, 664–670.